

**Properties of phonon modes of an ion-trap quantum computer in the Aubry phase**Justin Loye <sup>1,2</sup>, José Lages <sup>3</sup>, and Dima L. Shepelyansky <sup>2</sup><sup>1</sup>*Institut de Recherche en Informatique de Toulouse, Université de Toulouse, UPS, 31062 Toulouse, France*<sup>2</sup>*Laboratoire de Physique Théorique, IRSAMC, Université de Toulouse, CNRS, UPS, 31062 Toulouse, France*<sup>3</sup>*Institut UTINAM, OSU THETA, CNRS, Université Bourgogne Franche-Comté, 25010 Besançon, France*

(Received 10 February 2020; accepted 9 March 2020; published 30 March 2020)

We study analytically and numerically the properties of phonon modes in an ion quantum computer. The ion chain is placed in a harmonic trap with an additional periodic potential of which dimensionless amplitude  $K$  determines three main phases available for quantum computations: at zero  $K$  we have the case of Cirac-Zoller quantum computer, below a certain critical amplitude  $K < K_c$  the ions are in the Kolmogorov-Arnold-Moser (KAM) phase, with delocalized phonon modes and free chain sliding, and above the critical amplitude  $K > K_c$  ions are in the pinned Aubry phase with a finite frequency gap protecting quantum gates from temperature and other external fluctuations. For the Aubry phase, in contrast to the Cirac-Zoller and KAM phases, the phonon gap remains independent of the number of ions placed in the trap keeping a fixed ion density around the trap center. We show that in the Aubry phase the phonon modes are much better localized compared to the Cirac-Zoller and KAM cases. Thus in the Aubry phase the recoil pulses lead to local oscillations of ions, while in the other two phases they spread rapidly over the whole ion chains, making them rather sensible to external fluctuations. We argue that the properties of localized phonon modes and phonon gap in the Aubry phase provide advantages for the ion quantum computations in this phase with a large number of ions.

DOI: [10.1103/PhysRevA.101.032349](https://doi.org/10.1103/PhysRevA.101.032349)**I. INTRODUCTION**

The Cirac-Zoller 1995 proposal [1] initiated active experimental investigations of a quantum computer with cold ions in a trap oscillator potential. In the same year, a fundamental quantum logic gate had been experimentally realized [2], followed by realizations of entanglement, robust controlled-NOT quantum gates, and simple quantum algorithms with two to four qubits [3–6]. This initial stage of development of ion quantum computers is reviewed in [7,8]. The impressive progress in the quantum states control is highlighted in the Nobel lecture in [9].

In 2019, the ion quantum computers demonstrated an impressive boost with realizations of several quantum algorithms with up to 11 qubits [10–14]. Hybrid classical-quantum algorithms have even been realized with up to 20 qubits [15]. At present about 100 ions can be trapped and kept routinely for hours [16]. The review of the present experimental status on ion quantum computing is given in [17].

This remarkable progress of ion quantum computing makes the scalability problem of these computations of great actuality. Indeed, the Cirac-Zoller 1995 proposal [1] is not scalable for large  $N$ , since, at fixed average distance between ions, the trap frequency  $\omega_{tr}$  goes to zero as  $N \rightarrow \infty$ , and thus the quantum gates become very slow. Also, the coupling between ion chain and the internal ion levels drops as  $1/\sqrt{N}$ . To avoid these scaling problems for large  $N$ , it was proposed to place ions in the Aubry pinned phase created by an additional periodic potential [18]. In the Aubry phase, the phonon excitations of the ion chain have an excitation gap independent of  $N$  that is expected to protect the accuracy of quantum gates even for  $N \rightarrow \infty$ .

The first theoretical study of ions in a periodic potential had been reported in [19]. It was shown that this system can be locally described by the Frenkel-Kontorova model of particles connected by linear springs and placed in a periodic potential of amplitude  $K$  [20]. In this model, the equilibrium positions of the particles are described by the Chirikov standard map [21]. The physics of the model is understood from the properties of dynamical symplectic maps with invariant Kolmogorov-Arnold-Moser (KAM) curves at  $K < K_c$  and the fractal cantori replacing these KAM curves at  $K > K_c$ . The KAM phase corresponds to integrable dynamics while the cantori phase appears in the regime of chaotic dynamics [21–24]. As proved by Aubry [24], the cantori state corresponds to the minimal energy of particles. The Chirikov standard map provides a local description of various symplectic maps, and thus it describes a variety of physical systems [25] including the properties of an ion chain in a periodic potential.

At small potential amplitude  $K$ , the excitation of ions has an almost acoustic spectrum starting from the trap frequency  $\omega_{tr}$ , which goes to zero as  $N \rightarrow \infty$ . However, when the optical lattice amplitude  $K$  exceeds a certain critical value  $K_c$ , the chain enters in the Aubry pinned phase with the appearance of an excitation gap  $\omega_g$ , which is independent of the chain length and of the number of ions. The main properties of this charge system are described in [18,19,26,27]. However, these studies mainly addressed the transport properties of charges, while for the analysis of the robustness of the quantum gates it is necessary to understand the properties of phonon excitations of the ion chain and its response to the recoil momentum transfer from the laser pulses acting on internal ion states. Here, we present the detailed study of such phonon properties

performed with numerical simulations of the dynamics of 50 to 400 ions in the KAM and Aubry phases created by a periodic potential.

We also note that the experimental investigations of cold ions in a periodic potential have been started in [28,29] with the first signatures of the Aubry transition reported with five ions by the Vuletic group [30]. The experiments with a larger number of ions are now in progress [31,32] showing that the investigations of quantum computing in the Aubry phase are within the reach of state-of-the-art trapped cold ion techniques.

The paper is organized as follows: in Sec. II, we give the system description, the properties of phonon modes are analyzed in Sec. III, the properties of the recoil pulse propagation are described in Sec. IV, the glassy properties of low-energy ion chain configurations are depicted in Sec. V, and discussion of results and conclusion are given in Sec. VI. The Appendix provides additional complementary material.

## II. SYSTEM DESCRIPTION

The chain of ions in a one-dimensional periodic potential is described by the following Hamiltonian:

$$H = \sum_{i=1}^N \left( \frac{P_i^2}{2} + \omega_{\text{tr}}^2 \frac{x_i^2}{2} - K \cos x_i \right) + \sum_{i>j} \frac{1}{|x_i - x_j|}, \quad (1)$$

where  $x_i$  and  $P_i$  are the conjugated coordinate and momentum of the  $i$ th ion,  $\omega_{\text{tr}}$  is the frequency of the harmonic trap, and  $K$  is the amplitude of the optical array. The Hamiltonian is written in the following dimensionless units: the spatial period of the optical lattice is  $\ell = 2\pi$ , the ion mass is  $m = 1$ , the net atom charge is  $|Q| = 1$ , and the Coulomb constant is  $k_e = 1$ . In these atomic-type units, the physical parameters are measured in units of length  $r_a = \ell/2\pi$ , of energy  $\epsilon_a = k_e Q^2/r_a = 2\pi k_e Q^2/\ell$ , of electric-field strength  $E_a = \epsilon_a/(|Q|r_a)$ , of particle velocity  $v_a = \sqrt{\epsilon_a/m}$ , and of time  $t_a = r_a\sqrt{m/\epsilon_a}$ . For  $\ell = 1 \mu\text{m}$  and  $Q = e$ , the dimensionless temperature  $T = 0.01$  corresponds to the physical temperature  $T = \pi k_e Q^2/(50\ell k_B) \approx 1 \text{ K}$ . The dimensionless Planck constant is  $\hbar_{\text{eff}} = (\hbar/|Q|)\sqrt{2\pi/(k_e \ell m)} \sim 10^{-4}$  being very small for  $\ell \approx 1 \mu\text{m}$  and, e.g.,  $^{40}\text{Ca}^+$  ions. Since  $\hbar_{\text{eff}}$  is very small the ion dynamics can be considered as classical.

The equilibrium static positions of ions in a periodic potential are determined by the conditions  $\{\partial H/\partial x_i = 0, P_i = 0\}$  for all  $i = 1, \dots, N$  [19,24,27]. In the nearest-neighbor approximation for interacting ions, these conditions lead to the symplectic map giving the recurrence relation of equilibrium ion positions  $x_i$

$$p_{i+1} = p_i + Kg(x_i), \quad x_{i+1} = x_i + 1/\sqrt{p_{i+1}}, \quad (2)$$

where the effective momentum  $p_i = 1/(x_i - x_{i-1})^2$  is conjugated to  $x_i$  and the kick function is  $g(x) = -\sin x - (\omega^2/K)x$ . In [19,27], it is shown that this map (2) describes well the actual equilibrium ion positions even when all interactions between ions are taken into account. Let us define the average ion density  $\nu = N/L$ , where  $L$  is the number of spatial periods of the optical lattice. The map (2) can be locally linearized in order to obtain the Chirikov standard map. This procedure allows one to find the Aubry transition threshold

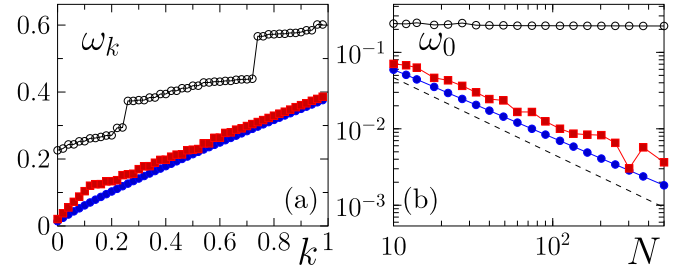


FIG. 1. (a) Spectrum of phonon excitations  $\omega_k$  as a function of the scaled mode number  $k = i/N$  ( $i = 0, \dots, N-1$ ). Here  $N = 50$ ,  $\nu \approx \nu_g$ , and  $\omega_{\text{tr}} = 0.014$ . (b) Evolution of the lowest phonon mode  $\omega_0$  as the number of ions  $N$  increases for  $\nu \approx \nu_g$ . For both panels blue dots, red squares, and black circles respectively correspond to the Cirac-Zoller case ( $K = 0$ ), the KAM case ( $K = 0.0154 \approx K_c/3$ ), and the Aubry case ( $K = 0.1386 \approx 3K_c$ ). The dashed line in panel (b) indicates the dependence  $\omega_0 = 0.47/N^b$  with  $b = 1$ ; the fit of blue points for the Cirac-Zoller case gives the exponent  $b = 0.892 \pm 0.00028$  [for the other cases the fit values of  $b$  are  $b = 0.743 \pm 0.023$  (KAM) and  $b = 0.0132 \pm 0.0026$  (Aubry)].

$K_c \approx 0.034(\nu/\nu_g)^3$  as a function of the average ion density. Here,  $\nu_g = 1.618\dots$  is the golden mean density at the central part of the chain [19,27]. For  $\nu = \nu_g$ , the numerical data gives  $K_c \approx 0.0462$  being close to the theoretical value.

## III. PROPERTIES OF PHONON EIGENMODES

The equilibrium ion positions are obtained numerically by the gradient method [24] and/or by the Metropolis algorithm described and already used in [19,26,27]. The main minimization procedure starts from the ground-state configuration at  $K = 0$  with subsequent step by step increase of  $K$  followed by energy minimization at each  $K$  (see also discussion below). We consider the case of ion density  $\nu \approx 1.618$  being fixed for the central part of the chain near the trap minimum. This ion density is equal to the rotation number  $\nu = N/L$ , i.e., along the chain,  $N$  ions are placed over  $L$  optical lattice periods. The  $\nu_g = (1 + \sqrt{5})/2 = 1.618\dots$  golden mean rotation number corresponds to the most robust KAM curve (see, e.g., Refs. [22,23]). This  $\nu_g$  value is taken as the average density of 1/3-central part of the whole chain. It can be tuned by a change of  $\omega_{\text{tr}}$ . Examples of ion positions for KAM and Aubry phases are given in Appendix Figs. 6 and 7 (see also [19,27]). The phase space of the map (2) and the equilibrium ion positions are shown in Appendix Fig. 8.

The Hamiltonian (1) is linearized for small ion oscillations near the equilibrium positions and then the phonon spectrum and eigenmodes are obtained by matrix diagonalization. Examples of phonon spectrum  $\omega(k)$  for the Cirac-Zoller case at  $K = 0$ , and for the KAM and the Aubry phases, are shown in Fig. 1. It is clear that for a large number of ions the minimal phonon frequency  $\omega_0$  goes to zero for the Cirac-Zoller case and the KAM phase. In contrast for the Aubry phase we have an optical type phonon gap with  $\omega_0 = \omega_g$  independent of the number of ions. Dependence of  $\omega_0$  on  $K$  is given in Appendix Fig. 9 (see similar cases in [19,27]).

Examples of eigenmodes  $\psi_k(x_i)$  with the two lowest frequencies ( $k = 0, 1$ ) are shown in Fig. 2. They clearly show

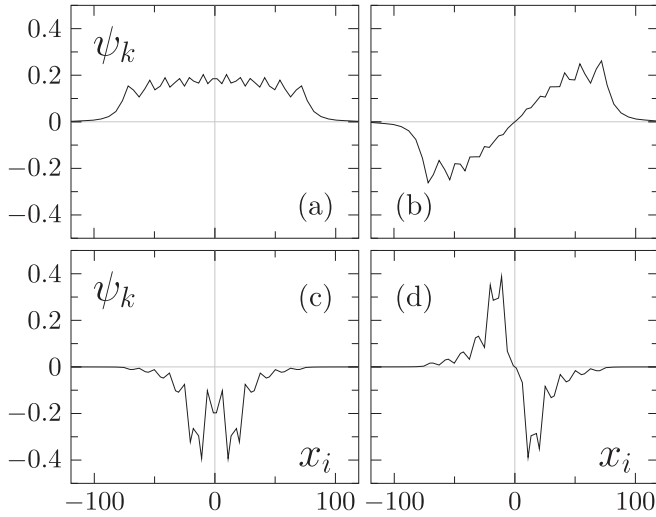


FIG. 2. Amplitude of eigenmodes  $\psi_k$  as a function of ion positions  $x_i$  for the KAM phase at  $K = 0.0154 \approx K_c/3$  (first row) and the Aubry phase at  $K = 0.1386 \approx 3K_c$  (second row), for  $k = 0$  (left column) and  $k = 1$  (right column). Here  $N = 50$ ,  $\nu \approx \nu_g$ , and  $\omega_{tr} = 0.014$ .

that for the KAM case ( $K < K_c$ ), and by extension for the Cirac-Zoller case ( $K = 0$ ), these modes are delocalized over the whole chain, while for the Aubry phase ( $K > K_c$ ) these modes are much more localized on a relatively small number of ions. A more quantitative measure of the eigenmode spreading over the chain can be obtained from the inverse participation ratio (IPR) defined for an eigenmode  $\psi_k$  as  $\xi_k = [\sum_i |\psi_k(i)|^2]^2 / \sum_i |\psi_k(i)|^4$ . This quantity is broadly used in condensed matter for systems with disorder and Anderson localization (see, e.g., Ref. [33]).

The IPR  $\xi_k$  is shown in Fig. 3 for the Cirac-Zoller case, the KAM phase, and the Aubry phase. The data shows that IPR values are significantly higher for the Cirac-Zoller and KAM cases compared to the Aubry case with the average values  $\bar{\xi} = \sum_k \xi_k / N = 20.001, 17.098, 6.148$ , re-

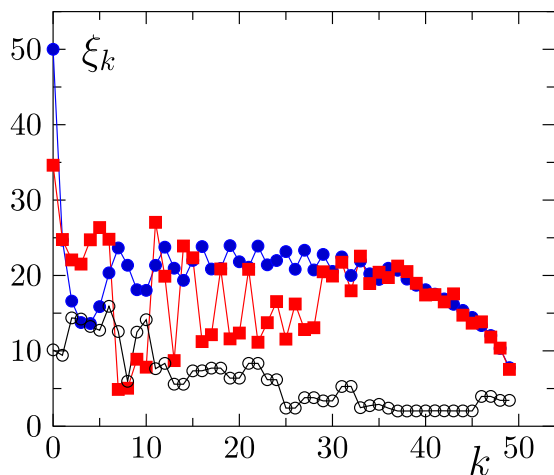


FIG. 3. Inverse participation ratio  $\xi_k$  as a function of mode index  $k$  for  $K = 0$  (blue dots),  $K = 0.0154 \approx K_c/3$  (red squares), and  $3K_c = 0.1386$  (black circles). Here  $N = 50$ ,  $\nu \approx \nu_g$ , and  $\omega_{tr} = 0.014$ .

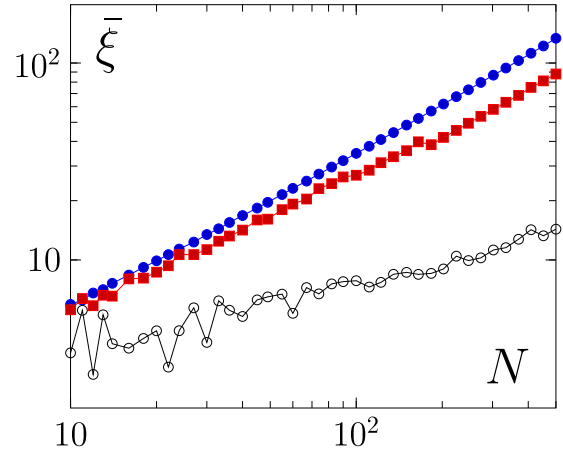


FIG. 4. Average inverse participation ratio  $\bar{\xi}$  as a function of number of ions for the Cirac-Zoller case  $K = 0$  (blue dots), KAM case  $K = 0.0154 \approx K_c/3$  (red squares), and the Aubry phase  $K = 0.1386 \approx 3K_c$  (black circles). The algebraic fit  $\bar{\xi} = aN^b$  for  $\omega_{tr} = 0.014$  gives respectively the value of exponent:  $b = 0.796 \pm 0.0029$  (Cirac-Zoller case),  $b = 0.696 \pm 0.0049$  (KAM case), and  $b = 0.349 \pm 0.021$  (Aubry case).

spectively, for  $N = 50$ . For higher  $N$  values we find respectively  $\bar{\xi} = 48.411, 35.173, 8.248$  (for  $N = 150$ ) and  $\bar{\xi} = 86.282, 58.063, 11.685$  (for  $N = 300$ ). Some higher eigenmodes are depicted in Appendix Fig. 10.

The dependence of  $\bar{\xi}$ , averaged over all modes on number of ions is shown in Fig. 4. This data clearly shows that in the limit of a large number of ions the Aubry case has much more localized modes compared to the Cirac-Zoller and KAM cases. Such localized modes are preferable for local quantum gates operation since local modes interactions between modes and ions are stronger and thus quantum gates are more rapid. Indeed, the more the modes are localized, the more the ion displacement amplitudes are large, and consequently the coupling with the driving laser is stronger. Also extended modes are expected to be more sensitive to various fluctuations. Thus, we argue that the localization of phonon modes is expected to be more favorable for operation of quantum gates generated by laser pulses acting locally on internal states of a specific ion.

#### IV. RECOIL PULSE DISINTEGRATION

The study of the eigenmodes allows one to understand the phonon properties of the ion chain. However, the realization of quantum gates involves the application of laser pulses which induce transitions between one-qubit states (formed by internal ion levels) and also induce interactions between qubits via ion recoil (see, e.g., Refs. [1,7,8]).

In Fig. 5, we present a numerical analysis of how an initial small recoil impulse  $\delta P_i$ , given to a selected ion  $i$  in the chain at equilibrium (ions at rest), propagates through the chain. The obtained results clearly show that for the Cirac-Zoller case the initial impulse rapidly spreads through the whole ion chain (top panel of Fig. 5). Indeed, in this case the recoil is transferred to the bus mode leading to harmonic oscillations of ion chain. This allows one to obtain interactions between

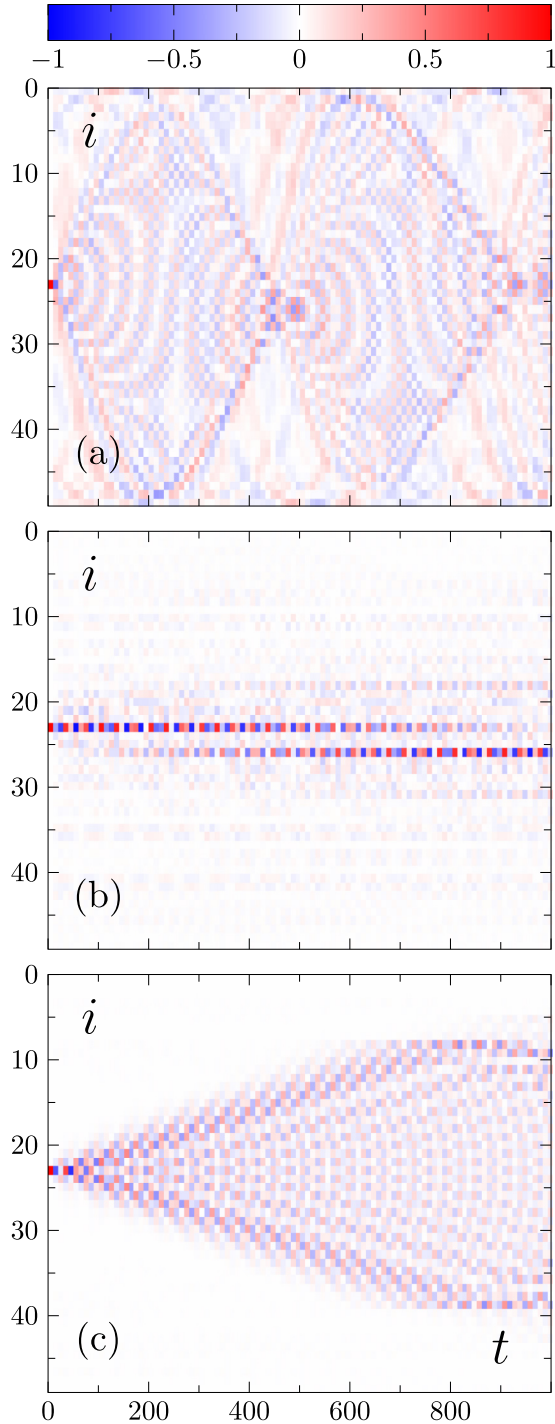


FIG. 5. Recoil pulse spreading over ion chain in time. The vertical axis shows ion number  $i$  and the horizontal axis shows the dimensionless time  $t$ . The initial momentum recoil  $\delta P_0 = 10^{-3}$  is given to ion  $i = 23$ , for the Cirac-Zoller case  $K = 0$  (top panel), the Aubry phase at  $K = 0.1386 \approx 3K_c$  with  $\nu \approx \nu_g$  (middle panel), and with integer density  $\nu \approx 1$  (bottom panel). Here  $N = 50$ . The color gives the relative ion momentum  $P_i/\delta P_0$ .

distant ion qubits. However, the matrix element of such an interaction drops as  $1/\sqrt{N}$  [see Eq. (2) in [1]]. Also the perturbative excitation of other modes leads to the propagation of perturbation all over the ion chain, as it is well visible in

Fig. 5. Such a perturbation disturbs the accuracy of quantum gates. A similar situation is observed for the KAM phase shown in Appendix Fig. 11.

The situation is qualitatively different for the Aubry phase. Here the recoil impulse remains mainly localized between nearby ions with a rather weak perturbation of other ions (middle panel of Fig. 5). Such a structure of recoil propagation allows one to create rapid two-qubit gates between nearby ion qubits. Indeed, the time scale of gate operation  $t_g$  is determined by the strong Coulomb interaction between nearby ions and by the periodic potential amplitude. We can estimate the two-qubit gate operation time to be  $t_g \propto 1/\omega_g$ . This time scale is independent of the number of ions  $N$  in contrast to the Cirac-Zoller case. Of course, these Aubry two-qubit gates in the Aubry phase are local, acting between nearby ion qubits, while for the Cirac-Zoller case the bus mode allows one in principle to create a two-qubit gate between distant ion qubits. However, the Cirac-Zoller gates are slow in comparison with the Aubry gates. Moreover, the broad spreading of recoil pulse over the whole chain (Fig. 5, top panel) will spoil rapidly the accuracy of such gates.

The advantage of the Cirac-Zoller proposal is the ability to construct slow but long-range gates. However, the coupling matrix element in such gates drops as  $1/\sqrt{N}$  and the minimal frequency of the gates also drops as  $\omega_0 \propto 1/N$  [see Fig. 1(b)]. Such gates are very slow and, thus, should be sensitive to various fluctuations present in the system. By contrast, in the Aubry phase, we can operate with gates acting mainly between nearby ions. The corresponding strength of interactions between nearby pinned ions is order of unity in the chosen dimensionless units (or  $\epsilon_a$  since Coulomb interactions are very strong between nearby ions). These gates are rapid, local, and thus they are expected to be much less sensitive to fluctuations. Of course, there is a certain disadvantage in the local nature of these gates since one will need to perform about  $N$  gates to couple qubits on opposite ends of the chain, but this feature is present almost for all configurations of quantum computers where the gates are assumed to be mainly local.

Above, we discussed the Aubry phase with ion density  $\nu \approx 1.618$ . At a first glance, one can suppose that it is possible to consider a much simpler case at  $\nu \approx 1$  when each lattice period contains only one ion (if one neglects boundary effects of the trap potential). In fact, a configuration of a similar type had been proposed by Cirac-Zoller in [34] where a periodic potential was assumed to be created by equidistant microtraps. However, it was argued [18] that for  $\nu = 1$ , even with a high periodic potential amplitude, Bloch waves will ballistically propagate through the whole periodic crystal-like structure according to the Bloch theorem [35,36]. The presence of such a Bloch wave at  $\nu \approx 1$  is clearly seen in Fig. 5 (bottom panel). The wave propagates through the system till times  $t \approx 500$ , leading to excitation of about half of all ions. Finally, for  $t > 500$  this propagation becomes bounded due to the presence of global harmonic trap with frequency  $\omega_{tr}$ , which breaks periodicity of ion chain at  $\nu \approx 1$  due to correction of ion local potential created by the global trap. Summarizing, for the  $\nu = 1$  case, a very large optical array amplitude  $K$ , inducing a strong pinning, produces an impulse propagation sharing similarities with the one associated to the Cirac-Zoller proposal.

The above result clearly shows that it is much more efficient to place ions in the Aubry phase at irrational density  $\nu$  where the recoil pulse propagation remains localized in the vicinity of the initially kicked ion. We suppose that the localization of phonon modes appears as a result of incommensurate ion density  $\nu$  that leads effectively to a certain type of Aubry-Andre incommensurate model [37], where a transition from metal phase (delocalized) to insulator phase (localized) appears with a variation of the hopping matrix element between lattice sites. In fact, the metal-insulator transition in the Aubry-Andre model has been observed in experiment with cold atoms in an optical lattice [38,39]. However, a verification of direct relation between localization of phonon modes in the Aubry phase and the Aubry-Andre model requires further more extended investigations.

### V. SPIN-GLASS PROPERTIES OF LOW-ENERGY CONFIGURATIONS OF AUBRY PHASE

The Aubry theorem [24] guarantees that the Cantori state with the fixed rotation number corresponding to the ion density provides the minimal energy ground state. However, in [19] it was shown that in fact there are exponentially many ion chain equilibrium configurations with energies exponentially close to the Aubry ground state. The number of such configurations is growing exponentially with the increase of the number of ions. Such a situation is similar to the case of spin-glass systems [40] (see also discussion in [18]). However, in the case of ion chain in a periodic potential there is no external randomness and in a sense we have here a dynamical spin-glass system where the spin-glass properties appear due to a dynamical chaos of the related symplectic map. The existence of many low-energy stable ion configurations means that it is rather difficult to reach the Aubry ground state in real experimental conditions. Above, we presented the results obtained with the minimization procedure with a step by step increase of  $K$  amplitude starting each energy minimization procedure with a previous step. We call this procedure the gradual step  $K$  increase minimization. Such a procedure can be realized experimentally by a slow increase of  $K$ . Other procedures can use also heating and cooling of an ion chain that can give other low-energy configurations. Thus a real experiment will most probably operate not with the absolute minimal Aubry ground state, but with a certain configuration with a local energy minimum being very close to the energy of the Aubry ground state. Consequently, it is important to ensure that these other configurations will also be characterized by a phonon gap. With the minimization procedure developed in [19], we determined about  $N_s = 200$  low-energy configurations for  $N = 50$  and  $N = 150$ . The energy histograms of these configurations are given in Appendix Fig. 12. For these  $N_s$  configurations we checked that all of them have approximately the same phonon gap, with an averaged width of  $\omega_0$ , and with an average variation being rather modest— $\delta\omega/\omega_g = [N_s^{-1} \sum_{N_s} (\omega_0 - \omega_{av})^2 / \omega_g^2]^{1/2} \approx 0.046$  for  $N = 50$  (see Appendix Fig. 13). We conclude that even if the experiment will not operate with ions in the lowest-energy configuration, still, the experimentally obtained low-energy configuration will have approximately the same properties as those

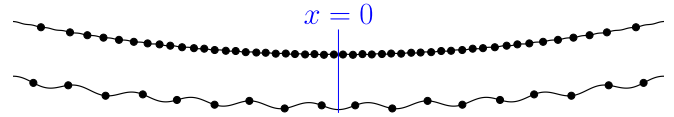


FIG. 6. Chain representation in the KAM phase ( $K = 0.0154 \approx K_c/3$ ). The black line shows the potential  $V(x) = \omega_w^2 x^2 / 2 - K \cos x$  and the black dots show the position of ions  $x_i$ . On the first line the whole chain is represented while on the second we zoom on the 17 central ions. Here  $N = 50$ ,  $\nu \approx \nu_g$ , and  $\omega_{tr} = 0.014$ . We highlight the center of the harmonic trap with a blue vertical line.

discussed above. Since the effective Planck constant is very small, the quantum tunneling between these configurations will take an enormously large time as discussed in [18,19]. On such a timescale, the ions can be considered as practically frozen (with only small oscillations induced by recoil effects).

### VI. DISCUSSION

The obtained results demonstrate a number of significant advantages of a quantum computer with ion qubit chain placed in the Aubry phase induced by an optical array. This phase is characterized by a firm gap for phonon excitations being independent of the number of ions. The phonon modes in this phase are much stronger localized on nearby ions compared to the delocalized modes of the Cirac-Zoller 1995 proposal [1]. As a result, a recoil laser pulse remains mainly localized between nearby ions that should allow the realization of rapid two-qubit gates between nearby ion qubits. These features open promising possibilities for a scalable ion quantum computer in the Aubry phase.

However, future detailed investigations of ions in the Aubry phase are highly desirable in order to directly numerically model the quantum gates taking into account both quantum nature of ion motion and its internal states.

The experimental investigations of ion quantum computer are within the reach of many experimental setups. Indeed, in [32], eight ions have been placed in a periodic potential of depth of  $T \approx 25$  mK. This depth is close to the Aubry transition at  $\nu \approx 0.38$  with  $K_c \approx 4 \times 10^{-4}$  and with a corresponding physical potential amplitude  $V_A \approx 40$  mK for  $\ell = 1 \mu\text{m}$  [27]. Thus we expect that the realization of two-qubit gates with ions in the Aubry phase can be performed with available experimental conditions.

Finally, we note that the Hamiltonian (1) can also be realized with electrons on a surface of liquid helium [41]. The experimental progress in a possible realization of such a system is reported in [42,43]. The efforts are also in progress [44] to realize a quantum computer with electrons on liquid helium as proposed in [45].

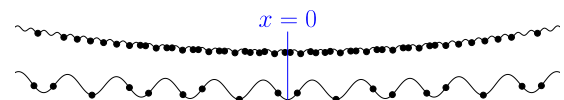


FIG. 7. Same as Fig. 6 for the Aubry phase ( $K = 0.1386 \approx 3K_c$ ).

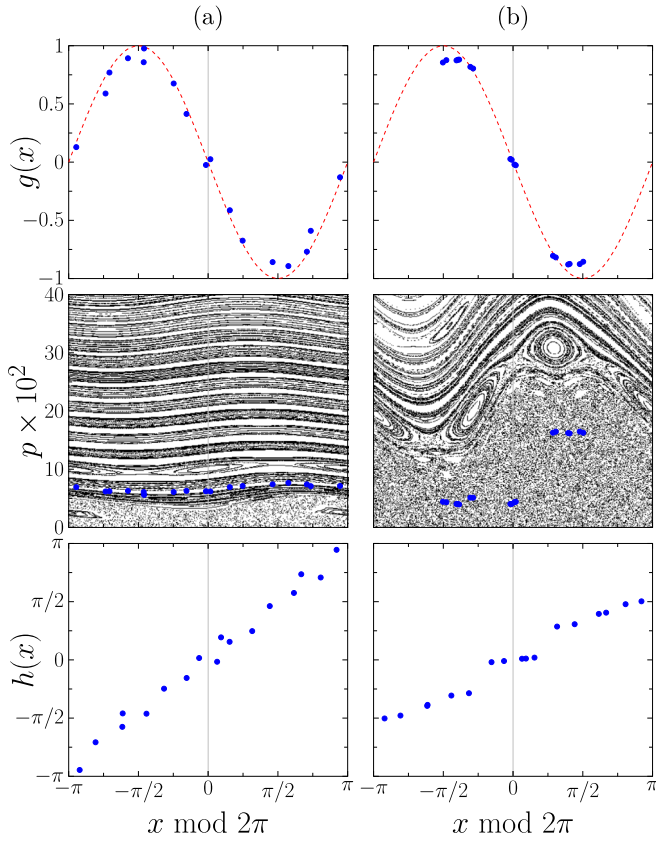


FIG. 8. Functions related to the ground state for  $K = 0.0154$  (KAM phase at left column) and  $K = 0.1386$  (Aubry phase at right column). Top row: the kick function  $g(x) = (p_{i+1} - p_i)/K$  obtained from the ion ground-state positions  $\{x_i\}_{i=N/3, \dots, 2N/3}$  (blue dots); the dashed curve shows the theoretical kick function  $g(x) = -\sin x$ . Central row: phase-space portrait of the map (2); blue dots show the points obtained from the equilibrium ion positions  $\{p_i, x_i\}_{i=N/3, \dots, 2N/3}$ . Bottom row: the hull function  $h(x)$  defined as the positions of the ions  $\{x_i\}_{i=N/3, \dots, 2N/3}$  versus their positions at  $K = 0$ . Here  $N = 50$ ,  $\nu = \nu_g \approx 1.618$ , and  $\omega_{tr} = 0.014$ .

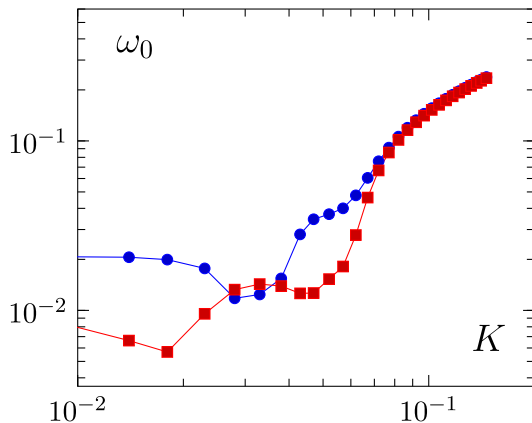


FIG. 9. Lowest phonon mode  $\omega_0$  as the periodic potential amplitude  $K$  increases for  $N = 50$  (blue dots) and  $N = 150$  (red squares). Here  $\nu = \nu_g$ .

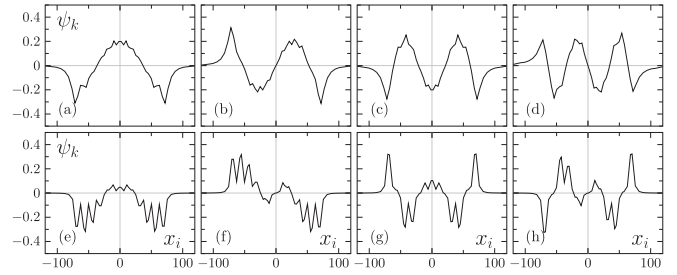


FIG. 10. Amplitude of eigenmodes  $\psi_k(i)$  as a function of ion positions  $x_i$  for KAM phase at  $K = 0.0154 \approx K_c/3$  (first row) and Aubry phase at  $K = 0.1386 \approx 3K_c$  (second row) for  $k = 2, 3, 4, 5$  (columns left to right). Here  $N = 50$ ,  $\nu \approx \nu_g$ , and  $\omega_{tr} = 0.014$ .

### ACKNOWLEDGMENTS

We thank O. V. Zhirov for useful discussions and advice for various energy minimization procedures. This work was supported in part by the Programme Investissements d'Avenir ANR-11-IDEX-0002-02, reference No. ANR-10-LABX-0037-NEXT (project THETRACOM). This work was also supported in part by the Programme Investissements d'Avenir ANR-15-IDEX-0003, ISITE-BFC (project GNET-WORKS), and in part by the Bourgogne Franche-Comté Region 2017-2020 APEX Project. Also this work was supported by APR 2019 call of University of Toulouse and by Region Occitanie (project GoIA).

### APPENDIX

Here we present supplementary figures 6, 7, 8, 9, 10, 11, 12, and 13 complementing the main text of

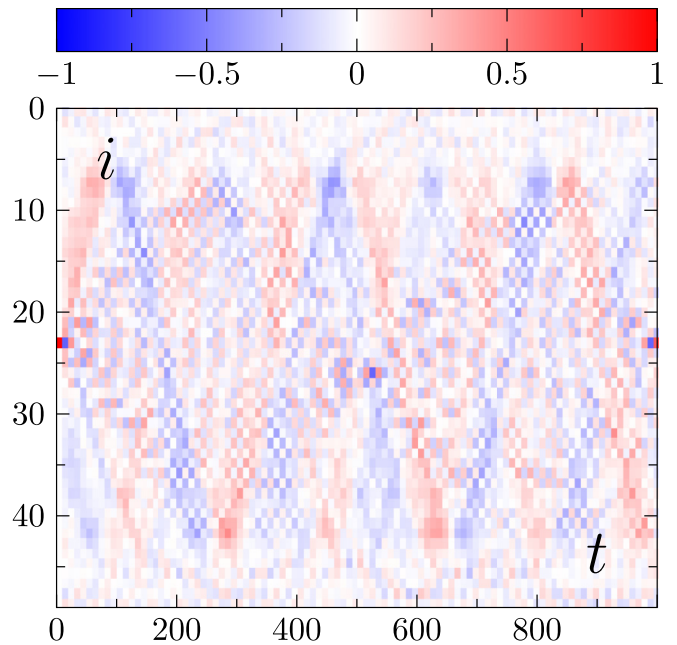


FIG. 11. Recoil pulse spreading over ion chain in time. The vertical axis shows ion number  $i$  and the horizontal axis shows dimensionless time  $t$ . The initial momentum recoil  $\delta P_0 = 10^{-3}$  is given to ion  $i = 23$  in the KAM phase  $K = 0.0154$ . Here  $N = 50$  and  $\omega_{tr} = 0.014$ . The color gives the relative ion momentum  $P_i/\delta P_0$ .

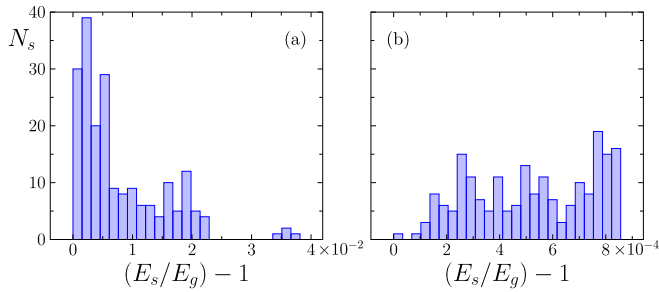


FIG. 12. Distribution histogram of fractions of  $N_s = 200$  energy lowest stable ion configurations over their energy  $E_s$  rescaled by the ground-state energy  $E_g$  (shown in the vertical axis). Here  $\omega_{tr} = 0.014$ ,  $N = 50$  (a) and  $\omega_{tr} = 0.005$ ,  $N = 150$  (b);  $K = 0.1386$ ,  $\nu \approx \nu_g$  in the central part of the ion chain.

the paper. We also add more detailed description of certain analytical results given in the main part of the article.

Figures 6 and 7 depict the equilibrium ion positions for KAM and Aubry phases.

The validity of the map description is illustrated in Fig. 8. Once the ground state of the chain is obtained, the equilibrium positions of the ions,  $\{x_1, \dots, x_N\}$ , can be used with the map (2) to obtain the successive values  $\{g(x_1), \dots, g(x_N)\}$  of the kick function  $g(x)$  (blue dots in the top row panels of Fig. 8). As expected these values lie on the top of the theoretical curve,  $g(x) = -\sin x$ , consequently validating the nearest-neighbor approximation used to derive the map (2). This validation is obtained for both the KAM phase (left column) and the Aubry phase (right column). More precisely the kick function is  $g(x) = -\sin x - (\omega^2/K)x$ , but we can neglect the harmonic contribution since its value is at most of the order of  $10^{-2}\pi$  for the KAM phase and of  $10^{-3}\pi$  for the Aubry phase. The map (2) describes the one-dimension dynamics of a fictitious particle which takes successive  $(x, p)$  positions in the phase space. The middle row panels of Fig. 8 give the phase-space portraits of the fictitious dynamics governed by the map (2). These phase-space portraits are obtained by iterating the map (2) from many initial conditions  $(x_0, p_0) \in [-\pi, \pi[ \times ]0, +\infty[$ . We observe that the ground-state positions are located on an invariant KAM curve for  $K < K_c$  (left column, KAM phase), and inside the chaotic component for  $K > K_c$  (right column, Aubry phase). The hull function  $h(x)$  shown in the bottom row panels of Fig. 8 is almost linear,  $h(x) \approx x$ , in the case of a sliding chain (left column, KAM phase), and  $h(x)$  exhibits a devil's staircase typical for a pinned chain (right column, Aubry phase). More information can be found in [26,27].

The dependence of the minimal phonon frequency  $\omega_0$  on potential amplitude  $K$  is shown in Fig. 9. For  $K < K_c$ , we have

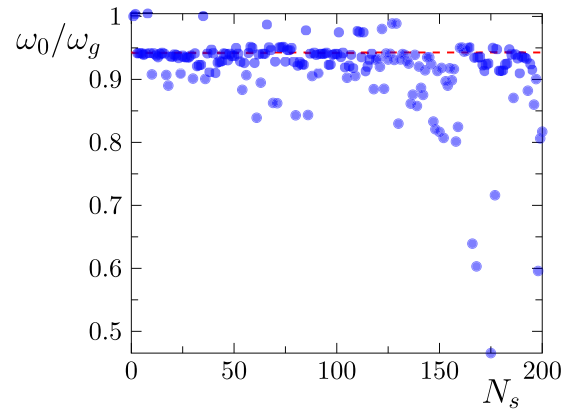


FIG. 13. Distribution of  $\omega_0/\omega_g$  for the  $N_s = 200$  lowest-energy configurations (ordered by energy starting from the ground state), where  $\omega_0$  is the lowest mode phonon frequency for the configurations and parameters of Fig. 12(a) and rescaling is done via the frequency  $\omega_g = 0.23969050023353308$  of the ground state obtained via minimization procedure described in [19]; dashed horizontal line marks the value of  $\omega_0 = 0.2259555158207294$  for the lowest-energy configuration found by the gradual step  $K$  increase minimization used in the main part of the article.

$\omega_0$  being close to zero and being practically independent of  $K$ . In contrast, for  $K > K_c$ , we have  $\omega_0$  being independent of the number of ions  $N$  with  $\omega_0$  growing with the increase of  $K$ .

A few high phonon eigenmodes are shown in Fig. 10.

The recoil pulse disintegration for the KAM phase is shown in Fig. 11.

The energy distributions of low-energy static ion configurations for  $N = 50$  and  $150$  are shown in Fig. 12. They are obtained with the minimization procedure described in [19]. The energy of the Aubry ground state obtained with this procedure is  $E_g = 55.314$ . It is slightly below the lowest-energy configuration obtained by the gradual  $K$  step increase minimization used for the figures of the main part of the article; this procedure gives the energy  $E_s = 55.560$ . We note that both these values are significantly below the lowest configuration energy obtained by the minimization procedure used in [28], which gives  $E_s = E_H = 55.681$  (for  $N = 150$  we have respectively the energies 216.956, 217.167, and 218.045). We think that the minimization used in [28] effectively forbids ion hopping between potential minima and due to that it is not able to find low-energy configurations. We think that it does not correspond to the reality of cold ion experiments where ions can hop from one potential well to another.

In Fig. 13, we show the variation of the lowest phonon frequency  $\omega_0$  of the  $N_s = 200$  lowest-energy configurations for  $N = 150$  ( $\omega_0$  is rescaled by  $\omega_g$ , which is the frequency  $\omega_0$  for the ground-state configuration).

- [1] J. I. Cirac and P. Zoller, Quantum Computations with Cold Trapped Ions, *Phys. Rev. Lett.* **74**, 4091 (1995).  
 [2] C. Monroe, D. M. Meekhof, B. E. King, W. N. Itano, and D. J. Wineland, Demonstration of a Fundamental Quantum Logic Gate, *Phys. Rev. Lett.* **75**, 4714 (1995).

- [3] C. A. Sackett, D. Kielpinski, B. E. King, C. Langer, V. Meyer, C. J. Myatt, M. Rowe, Q. A. Turchette, W. M. Itano, D. J. Wineland, and C. Monroe, Experimental entanglement of four particles, *Nature (London)* **404**, 256 (2000).

- [4] B. DeMarco, A. Ben-Kish, D. Leibfried, V. Meyer, M. Rowe, B. M. Jelenkovic, W. M. Itano, J. Britton, C. Langer, T. Rosenband, and D. J. Wineland, Experimental Demonstration of a Controlled-NOT Wave-Packet Gate, *Phys. Rev. Lett.* **89**, 267901 (2002).
- [5] D. Leibfried, B. DeMarco, V. Meyer, D. Lucas, M. Barrett, J. Britton, W. M. Itano, B. Jelenkovic, C. Langer, T. Rosenband, and D. J. Wineland, Experimental demonstration of a robust, high-fidelity geometric two ion-qubit phase gate, *Nature (London)* **422**, 412 (2003).
- [6] F. Schmidt-Kaler, H. Haffner, M. Riebe, S. Gulde, G. P. T. Lancaster, T. Deuschle, C. Becher, C. F. Roos, J. Eschner, and R. Blatt, Realization of the Cirac-Zoller controlled-NOT quantum gate, *Nature (London)* **422**, 408 (2003).
- [7] H. Haffner, C. F. Roos, and R. Blatt, Quantum computing with trapped ions, *Phys. Rep.* **469**, 155 (2008).
- [8] R. Blatt and C. F. Roos, Quantum simulations with trapped ions, *Nat. Phys.* **8**, 277 (2012).
- [9] D. J. Wineland, Nobel Lecture: Superposition, entanglement, and raising Schrodinger's cat, *Rev. Mod. Phys.* **85**, 1103 (2013).
- [10] Y. Nam, J.-S. Chen, N. C. Pinti, K. Wright, C. Delaney, D. Maslov, K. R. Brown, S. Allen, J. M. Amini, J. Apisdorf, K. M. Beck, A. Blinov, V. Chaplin, M. Chmielewski, C. Collins, S. Debnath, A. M. Ducore, K. M. Hudek, M. Keesan, S. M. Kreikemeier, J. Mizrahi, P. Solomon, M. Williams, J. D. Wong-Campos, C. Monroe, and J. Kim, Ground-state energy estimation of the water molecule on a trapped ion quantum computer, [arXiv:1902.10171](https://arxiv.org/abs/1902.10171) [quant-ph].
- [11] K. A. Landsman, C. Figgatt, T. Schuster, N. M. Linke, B. Yoshida, N. Y. Yao, and C. Monroe, Verified quantum information scrambling, *Nature (London)* **567**, 61 (2019).
- [12] K. Wright, K. M. Beck, S. Debnath, J. M. Amini, Y. Nam, N. Grzesiak, J.-S. Chen, N. C. Pinti, M. Chmielewski, C. Collins, K. M. Hudek, J. Mizrahi, J. D. Wong-Campos, S. Allen, J. Apisdorf, P. Solomon, M. Williams, A. M. Ducore, A. Blinov, S. M. Kreikemeier, V. Chaplin, M. Keesan, C. Monroe, and J. Kim, Benchmarking an 11-qubit quantum computer, *Nat. Commun.* **10**, 5464 (2019).
- [13] O. Shehab, K. Landsman, Y. Nam, D. Zhu, N. M. Linke, M. Keesan, R. C. Pooser, and C. Monroe, Toward convergence of effective field theory simulations on digital quantum computers, *Phys. Rev. A* **100**, 062319 (2019).
- [14] T. Brydges, A. Elben, P. Jurcevic, B. Vermersch, C. Maier, B. P. Lanyon, P. Zoller, R. Blatt, and C. F. Roos, Probing Renyi entanglement entropy via randomized measurements, *Science* **364**, 260 (2019).
- [15] C. Kokail, C. Maier, R. van Bijnen, T. Brydges, M. K. Joshi, P. Jurcevic, C. A. Muschik, P. Silvi, R. Blatt, C. F. Roos, and P. Zoller, Self-verifying variational quantum simulation of lattice models, *Nature (London)* **569**, 355 (2019).
- [16] G. Pagano, P. W. Hess, H. B. Kaplan, W. L. Tan, P. Richerme, P. Becker, A. Kyrianiadis, J. Zhang, E. Birkelbaw, M. R. Hernandez, Y. Wu, and C. Monroe, Cryogenic trapped-ion system for large scale quantum simulation, *Quantum Sci. Technol.* **4**, 014004 (2018).
- [17] C. D. Bruzewicz, J. Chiaverini, R. McConnel, and J. M. Sage, Trapped-ion quantum computing: progress and challenges, *Appl. Phys. Rev.* **6**, 021314 (2019).
- [18] D. L. Shepelyansky, Quantum computer with cold ions in the Aubry pinned phase, *Eur. Phys. J. D* **73**, 148 (2019).
- [19] I. Garcia-Mata, O. V. Zhirov, and D. L. Shepelyansky, Frenkel-Kontorova model with cold trapped ions, *Eur. Phys. J. D* **41**, 325 (2007).
- [20] O. M. Braun and Yu. S. Kivshar, *The Frenkel-Kontorova Model: Concepts, Methods, Applications* (Springer-Verlag, Berlin, 2004).
- [21] B. V. Chirikov, A universal instability of many-dimensional oscillator systems, *Phys. Rep.* **52**, 263 (1979).
- [22] A. J. Lichtenberg and M. A. Lieberman, *Regular and Chaotic Dynamics* (Springer, Berlin, 1992).
- [23] J. D. Meiss, Symplectic maps, variational principles, and transport, *Rev. Mod. Phys.* **64**, 795 (1992).
- [24] S. Aubry, The twist map, the extended Frenkel-Kontorova model and the devil's staircase, *Physica D* **7**, 240 (1983).
- [25] B. Chirikov and D. Shepelyansky, Chirikov standard map, *Scholarpedia* **3**, 3550 (2008).
- [26] O. V. Zhirov, and D. L. Shepelyansky, Thermoelectricity of Wigner crystal in a periodic potential, *Europhys. Lett.* **103**, 68008 (2013).
- [27] O. V. Zhirov, J. Lages, and D. L. Shepelyansky, Thermoelectricity of cold ions in optical lattices, *Eur. Phys. J. D* **73**, 149 (2019).
- [28] T. Pruttivarasin, M. Ramm, I. Talukdar, A. Kreuter, and H. Haffner, Trapped ions in optical lattices for probing oscillator chain models, *New J. Phys.* **13**, 075012 (2011).
- [29] A. Bylinskii, D. Gangloff, and V. Vuletic, Tuning friction atom-by-atom in an ion-crystal simulator, *Science* **348**, 1115 (2015).
- [30] A. Bylinskii, D. Gangloff, I. Countis, and V. Vuletic, Observation of Aubry-type transition in finite atom chains via friction, *Nat. Mater.* **15**, 717 (2016).
- [31] J. Kiethe, R. Nigmatullin, D. Kalincev, T. Schmirander, and T. E. Mehlstaubler, Probing nanofriction and Aubry-type signatures in a finite self-organized system, *Nat. Commun.* **8**, 15364 (2017).
- [32] T. Laupretre, R. B. Linnet, I. D. Leroux, H. Landa, A. Dantan, and M. Drewsen, Controlling the potential landscape and normal modes of ion Coulomb crystals by a standing-wave optical potential, *Phys. Rev. A* **99**, 031401(R) (2019).
- [33] E. Akkermans and G. Montambaux, *Mesoscopic Physics of Electrons and Photons* (Cambridge University Press, Cambridge, UK, 2007).
- [34] J. I. Cirac and P. Zoller, A scalable quantum computer with ions in an array of microtraps, *Nature (London)* **404**, 579 (2000).
- [35] F. Z. Bloch, Über die quantenmechanik der elektronen in kristallgittern, *Z. Phys.* **52**, 555 (1928).
- [36] C. Kittel, *Introduction to Solid State Physics* (Wiley, New York, 1996).
- [37] S. Aubry and G. Andre, Analyticity breaking and Anderson localization in incommensurate lattices, *Ann. Israel Phys. Soc.* **3**, 133 (1980).
- [38] G. Roati, C. D'Errico, L. Fallani, M. Fattori, C. Fort, M. Zaccanti, G. Modugno, M. Modugno, and M. Inguscio, Anderson localization of a non-interacting Bose-Einstein condensate, *Nature (London)* **453**, 895 (2008).
- [39] M. Schreiber, S. S. Hodgman, P. Bordia, H. Luschen, M. H. Fischer, R. Vosk, E. Altman, U. Schneider, and I. Bloch, Observation of many-body localization of interacting fermions in a quasirandom optical lattice, *Science* **349**, 842 (2015).
- [40] N. Mezard, G. Parisi, and M. A. Virasoro, *Spin Glass Theory and Beyond* (World Scientific, Singapore, 1997).

- [41] Y. Monarkha and K. Kono, *Two-Dimensional Coulomb Liquids and Solids* (Springer-Verlag, Berlin, 2004).
- [42] D. G.-Rees, S.-S. Yeh, B.-C. Lee, K. Kono, and J.-J. Lin, Bistable transport properties of a quasi-one-dimensional Wigner solid on liquid helium under continuous driving, *Phys. Rev. B* **96**, 205438 (2017).
- [43] J.-Y. Lin, A. V. Smorodin, A. O. Badrutdinov, and D. Konstantinov, Transport properties of a quasi-1D Wigner solid on liquid helium confined in a microchannel with periodic potential, *J. Low Temp. Phys.* **195**, 289 (2019).
- [44] E. Kawakami, A. Elarabi, and D. Konstantinov, Image-Charge Detection of the Rydberg States of Surface Electrons on Liquid Helium, *Phys. Rev. Lett.* **123**, 086801 (2019).
- [45] P. M. Platzman and M. I. Dykman, Quantum computing with electrons floating on liquid helium, *Science* **284**, 1967 (1999).